WRF v.3.9 sensitivity to land surface model and horizontal resolution changes over North America

Almudena García-García[1,2], Francisco José Cuesta-Valero[1], Hugo Beltrami[1], Fidel González-Rouco[3], and Elena García-Bustamante[4]

[1]Climate & Atmospheric Sciences Institute, St. Francis Xavier University, Antigonish, Nova Scotia, Canada
[2] Department of Remote Sensing, Helmholtz Centre for Environmental Research – UFZ, Leipzig, Germany
[3]Physics of the Earth and Astrophysics Department, IGEO (UCM-CSIC), Universidad Complutense de Madrid, Spain.
[4]Research Center for Energy, Environment and Technology (CIEMAT), Madrid, Spain.

Correspondence: Hugo Beltrami (hugo@stfx.ca)

Table S1. Pearson spatial correlation coefficients between anomalies of the surface energy fluxes (Figure 3 in the manuscript) and anomalies of near-surface temperatures (Figure 4 in the manuscript). Values of p < 0.01 are considered significant and marked in bold.

	CLM4			NOAH			NOAH-MP			NOAH-MP-DV		
	Annual	DJF	JJA	Annual	DJF	JJA	Annual	DJF	JJA	Annual	DJF	JJA
Maximum temperature												
SNET	**0.88**	**0.70**	**0.88**	**0.82**	**0.62**	**0.84**	**0.87**	**0.77**	**0.85**	**0.89**	**0.74**	**0.87**
LNET	**-0.75**	**-0.54**	**-0.90**	**-0.66**	**-0.21**	**-0.84**	**-0.62**	**-0.63**	**-0.73**	**-0.42**	**-0.64**	**-0.67**
RNET	**0.76**	**0.54**	**0.72**	**0.65**	**0.46**	**0.61**	**0.80**	**0.66**	**0.74**	**0.84**	**0.50**	**0.77**
GHF	0.01	**0.04**	**-0.28**	0.11	0.01	0.04	0.06	**-0.24**	**-0.22**	**-0.27**	**-0.18**	**-0.12**
HFX	**0.73**	**0.43**	**0.84**	**0.76**	**0.65**	**0.70**	**0.81**	**0.67**	**0.74**	**0.77**	**0.44**	**0.74**
Minimum Temperature												
SNET	**0.34**	**0.19**	**0.30**	**0.50**	**0.26**	**0.54**	**0.69**	**0.61**	**0.70**	**0.56**	**0.40**	**0.45**
LNET	**-0.67**	**-0.39**	**-0.32**	**-0.54**	**-0.12**	**-0.67**	**-0.65**	**-0.58**	**-0.66**	**-0.82**	**-0.49**	**-0.69**
RNET	**0.08**	0.01	**0.23**	**0.31**	**0.18**	**0.30**	**0.56**	**0.48**	**0.57**	**0.24**	**0.18**	**0.14**
GHF	**-0.30**	**0.03**	**-0.19**	0.02	**-0.50**	0.07	**0.13**	**-0.56**	**-0.15**	**0.14**	**-0.44**	**0.09**
HFX	0.01	**-0.19**	**0.07**	**0.20**	-0.01	**0.27**	**0.54**	**0.26**	**0.48**	**0.20**	**-0.10**	**0.11**
Soil Temperature at 1 m												
SNET	**0.52**	**0.17**	**0.56**	**0.55**	**0.26**	**0.42**	**0.77**	**0.32**	**0.58**	**0.37**	**0.21**	**0.47**
LNET	**-0.62**	**-0.49**	**-0.51**	**-0.51**	0.12	**-0.59**	**-0.65**	**-0.20**	**-0.57**	**-0.85**	**-0.41**	**-0.73**
RNET	**0.35**	-0.06	**0.51**	**0.40**	**0.28**	**0.18**	**0.66**	**0.30**	**0.45**	0.00	0.01	**0.14**
GHF	**0.02**	-0.01	-0.02	0.00	**-0.50**	**-0.20**	**-0.15**	**-0.66**	**-0.39**	**0.05**	**-0.52**	0.01
HFX	**0.28**	**-0.14**	**0.42**	**0.38**	**0.12**	**0.40**	**0.56**	**0.12**	**0.52**	0.02	**-0.25**	**0.18**

Table S2. Spatial correlation coefficients between anomalies of the surface energy fluxes (Figure 3 in the manuscript) and anomalies of near-surface humid conditions (Figure 5 in the manuscript). Correlation coefficients with the difference between total precipitation and evaporation (LH in mm/day units, PR-ETOT) were included for completeness. Values of p < 0.01 are considered significant and marked in bold.

	CLM4			NOAH			NOAH-MP			NOAH-MP-DV		
	Annual	DJF	JJA	Annual	DJF	JJA	Annual	DJF	JJA	Annual	DJF	JJA
Convective Precipitation												
RNET	-0.04	-0.22	0.12	-0.04	-0.17	0.10	0.21	0.13	0.04	0.24	0.10	0.15
LH	0.02	**0.21**	0.02	**0.11**	**0.27**	**0.08**	**0.14**	0.03	0.06	**0.15**	**0.14**	**0.20**
TCLDFR	-0.01	-0.02	**0.02**	**0.11**	-0.05	**0.09**	**-0.23**	**0.04**	**-0.08**	-0.02	**0.07**	**0.09**
PR-ETOT	**0.43**	**0.06**	**0.58**	**0.24**	-0.05	**0.54**	**0.05**	**0.11**	**0.04**	**-0.07**	-0.01	**0.18**
Non Convective Precipitation												
RNET	**-0.19**	**0.20**	**-0.45**	-0.05	**0.14**	**-0.18**	**0.13**	**0.10**	-0.03	**0.13**	**0.25**	**-0.18**
LH	**0.11**	**0.16**	**0.26**	**0.33**	**0.11**	**0.30**	**0.17**	**0.20**	**0.13**	0.166	**0.31**	**0.12**
TCLDFR	**0.60**	**0.66**	**0.67**	**0.59**	**0.60**	**0.41**	**0.34**	**0.68**	**0.22**	**0.50**	**0.54**	**0.41**
PR-ETOT	**0.17**	-0.01	**0.35**	**0.42**	**0.39**	**0.42**	**-0.09**	0.02	**0.23**	**0.08**	**0.04**	**0.17**
Soil Moisture content in the 1st soil meter												
RNET	**0.06**	0.00	**0.03**	**-0.19**	**-0.11**	**-0.37**	-0.05	-0.03	**-0.16**	**-0.11**	**-0.07**	**-0.18**
LH	**0.12**	**0.14**	0.02	-0.01	0.00	**-0.12**	-0.03	-0.01	**-0.14**	**-0.10**	-0.04	**-0.09**
TCLDFR	**-0.06**	0.01	**-0.06**	-0.05	-0.09	**0.18**	**0.20**	**0.07**	**0.22**	-0.03	0.01	**0.04**
PR-ETOT	**-0.25**	**-0.26**	**-0.07**	**0.25**	**0.21**	**0.15**	**0.20**	**0.19**	**0.12**	**0.25**	**0.24**	**0.10**
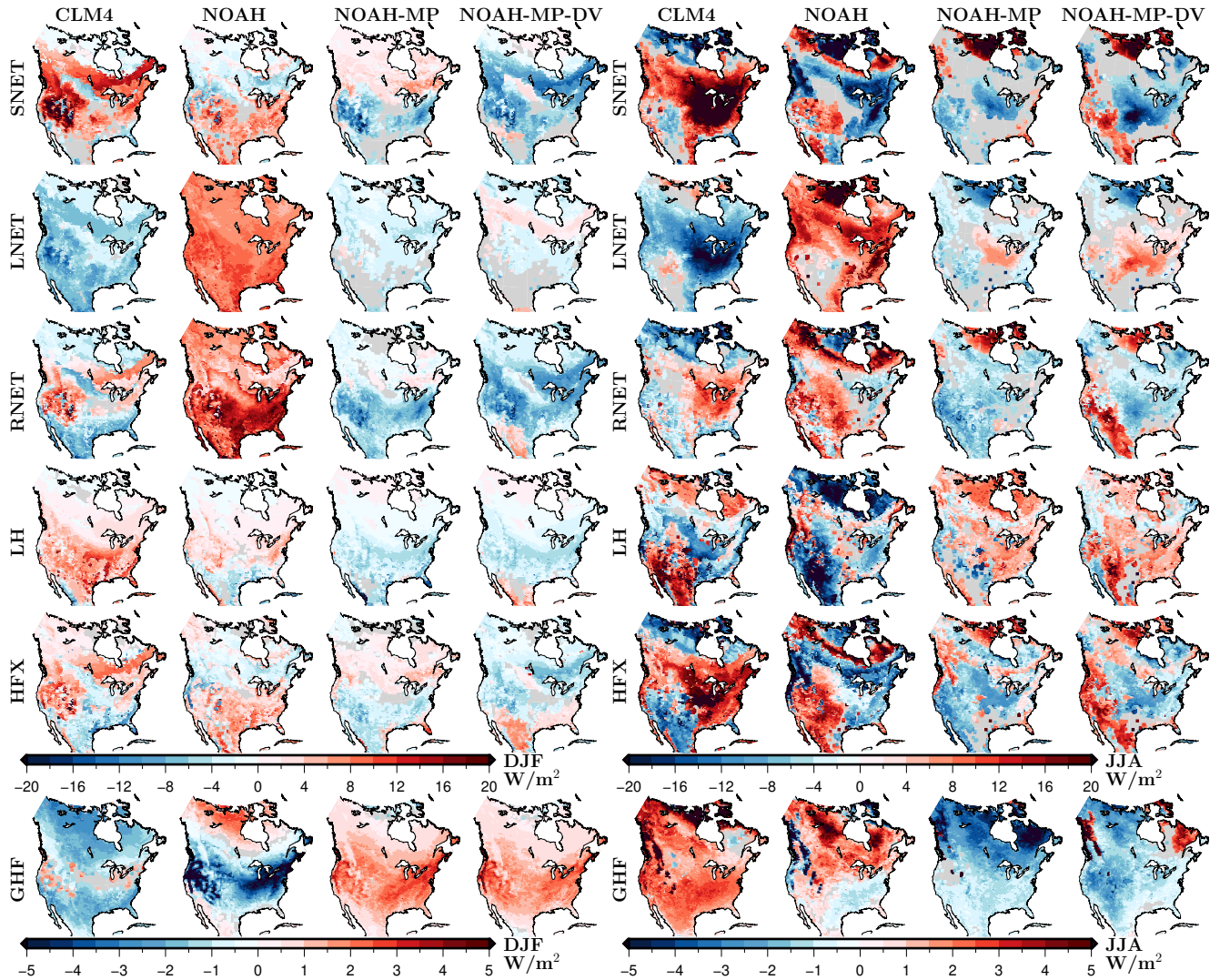
Figure S1. DJF (left) and JJA (right) anomalies of energy fluxes at the surface (net shortwave radiation SNET; net longwave radiation LNET; soil net radiation RNET; latent heat flux LH; sensible heat flux HFX; and ground heat flux GHF) for each LSM simulation relative to the LSM ensemble mean. Only grid cells with a significant change at the 5% significant level are plotted. Mean values are estimated as the temporal average for the period 1980-2013 using simulations performed with 50 km resolution.
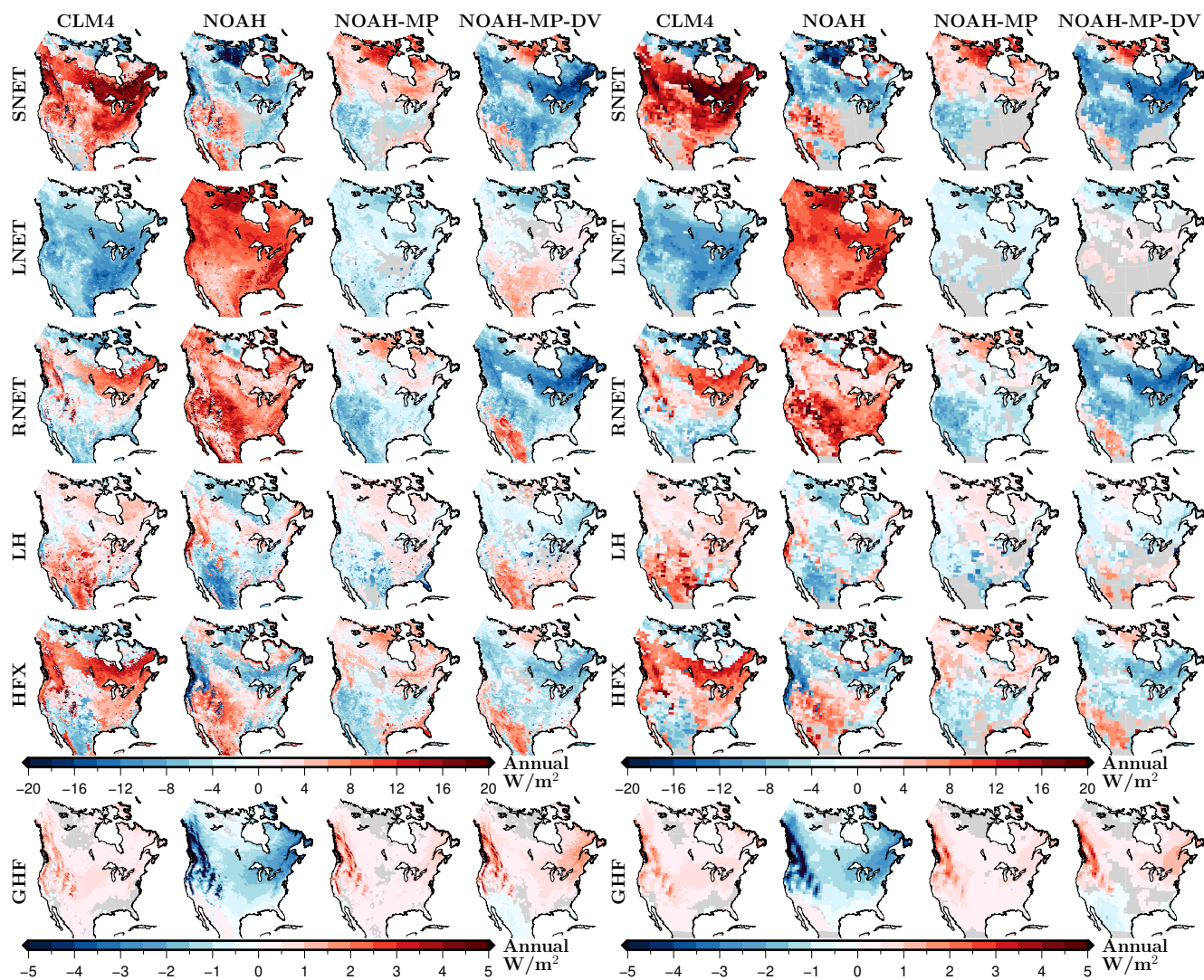
Figure S2. Annual anomalies of energy terms at the surface (net shortwave radiation SNET; net longwave radiation LNET; soil net radiation RNET; latent heat flux LH; sensible heat flux HFX; and ground heat flux GHF) for each LSM simulation relative to the LSM ensemble mean for each energy term. Grid cells with a non-significant change at the 5% significant level are masked in grey. Mean values are estimated as the temporal average for the period 1980-2013 using simulations performed with 25 km resolution (left) and 100 km resolution (right).
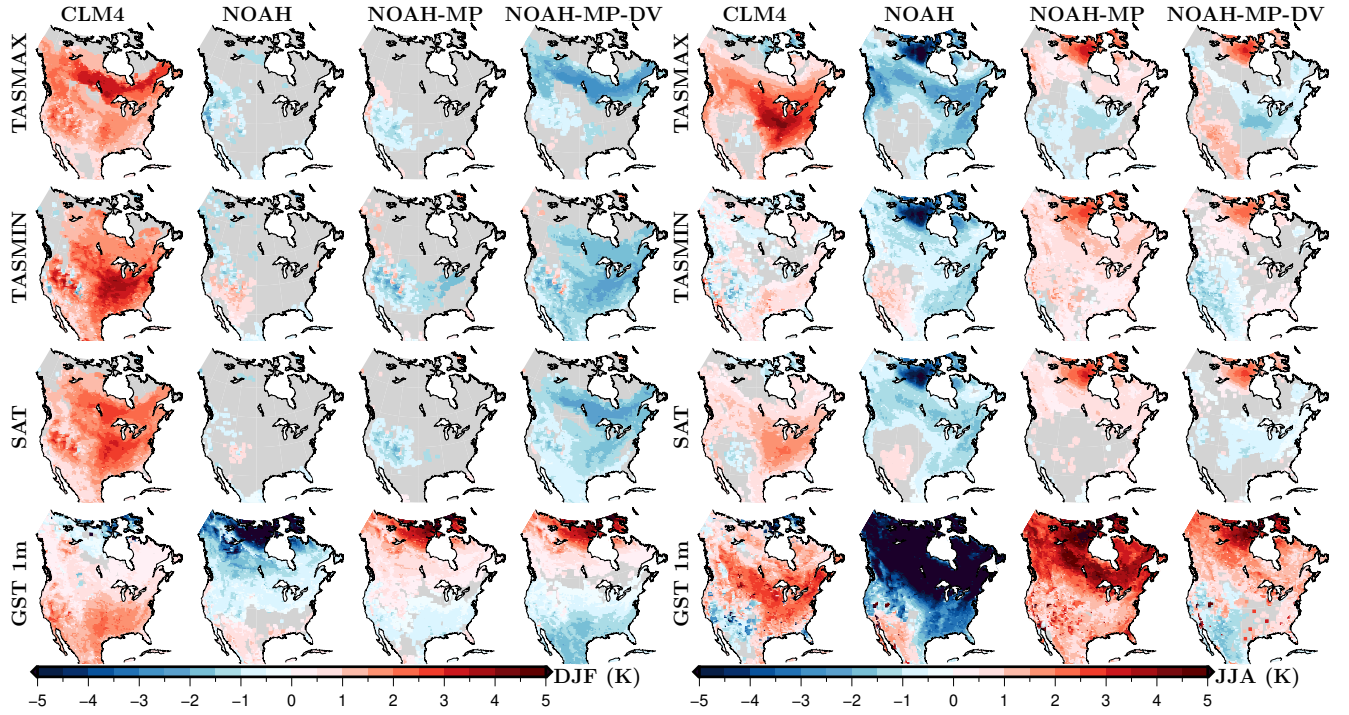
Figure S3. DJF (left) and JJA (right) anomalies of near-surface temperature conditions (maximum temperature TASMAX; minimum temperature TASMIN; surface air temperature SAT; and soil temperature at 1m depth GST 1m) for each LSM simulation relative to the LSM ensemble mean for each temperature term. Grid cells with a non-significant change at the 5% significant level are masked in grey. Mean values are estimated as the temporal average for the period 1980-2013 using simulations performed with 50 km resolution.
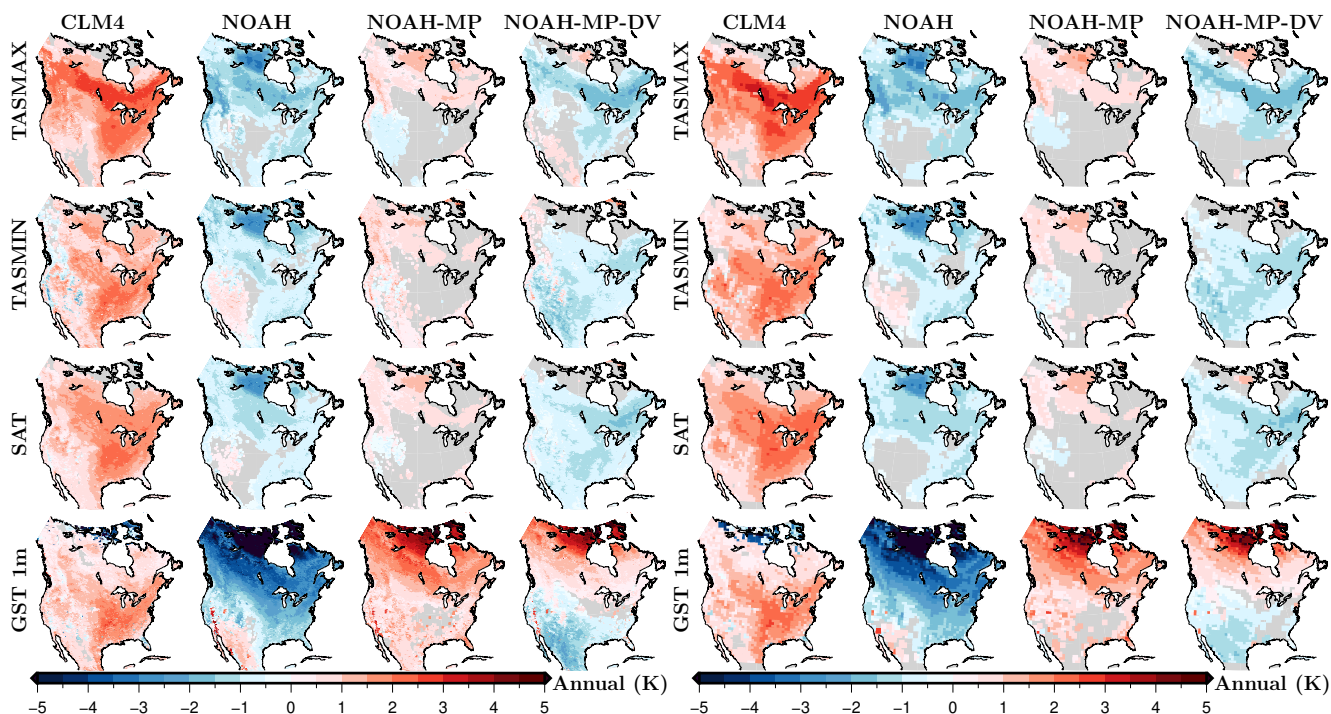
Figure S4. Annual anomalies of near-surface temperature conditions (maximum temperature TASMAX; minimum temperature TASMIN; surface air temperature SAT; and soil temperature at 1m depth GST 1m) for each LSM simulation relative to the LSM ensemble mean for each temperature term. Grid cells with a non-significant change at the 5% significant level are masked in grey. Mean values are estimated as the temporal average for the period 1980-2013 using simulations performed with 25 km resolution (left) and 100 km resolution (right).
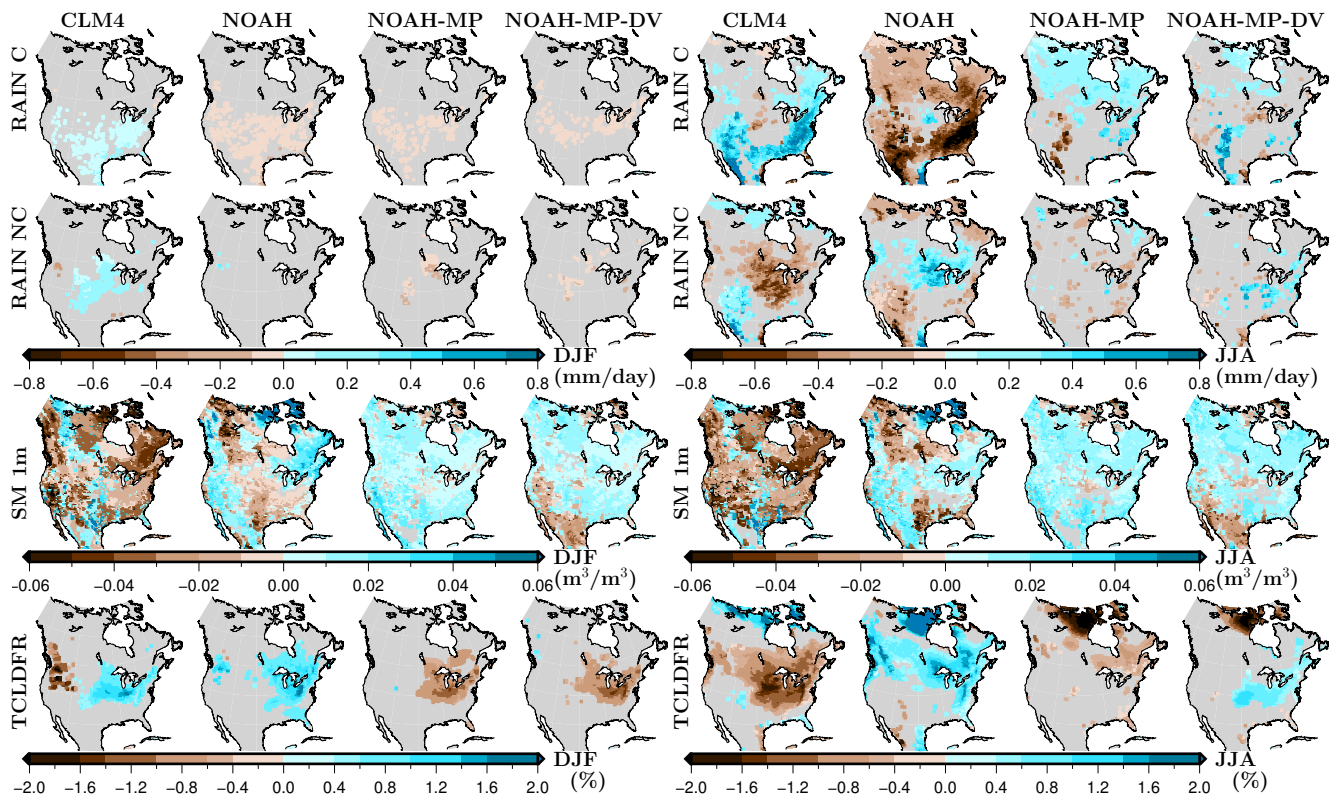
Figure S5. DJF (left) and JJA (right) anomalies of near-surface humid conditions (accumulated precipitation at the surface PRE; soil moisture contained in the first soil meter SM 1m; and total cloud fraction TCLDFR) for each LSM simulation relative to the LSM ensemble mean for each energy term. Grid cells with a non-significant change at the 5% significant level are masked in grey. Mean values are estimated as the temporal average for the period 1980-2013 using simulations performed with 50 km resolution.
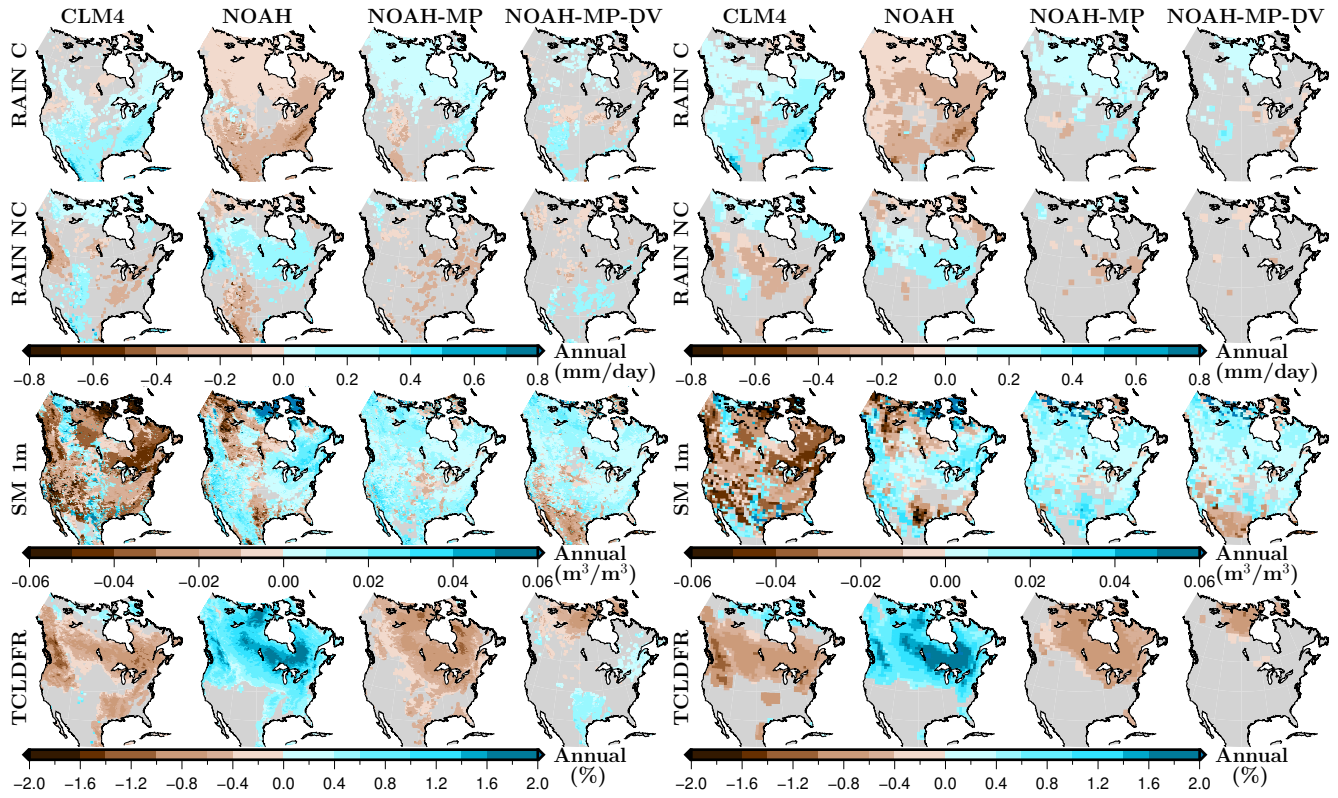
Figure S6. Annual anomalies of near-surface humid conditions (accumulated precipitation at the surface PRE; soil moisture contained in the first soil meter SM 1m; and total cloud fraction TCLDFR) for each LSM simulation relative to the LSM ensemble mean for each energy term. Grid cells with a non-significant change at the 5% significant level are masked in grey. Mean values are estimated as the temporal average for the period 1980-2013 using simulations performed with 25 km resolution (left) and 100 km resolution (right).
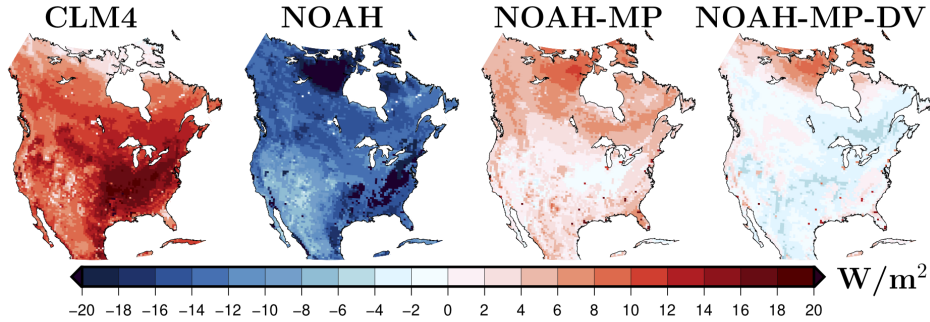
Figure S7. Anomalies of the outgoing component of the longwave radiation at the ground surface for each LSM simulation relative to the LSM ensemble mean. Mean values are estimated as the temporal average for the period 1980-2013 using simulations performed with 50 km resolution.
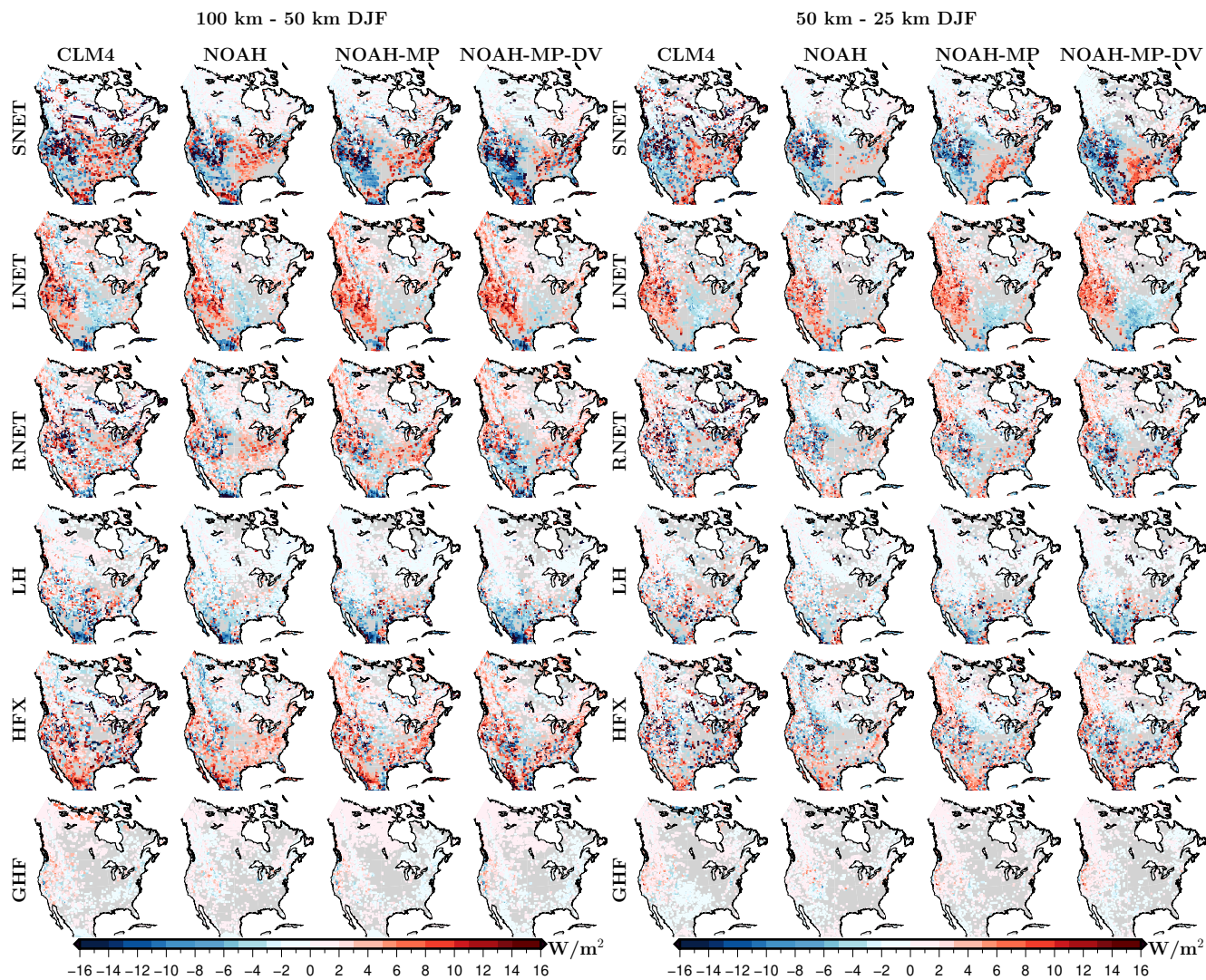
Figure S8. DJF mean difference in surface energy fluxes between the 100 km and 50 km simulations (left) and between the 50 km and 25 km simulations (right). Grid cells with a non-significant change at the 5% significant level are masked in grey. All outputs from the 25, 50 and 100 km simulations were mapped to a common grid (CRU grid) using the nearest model grid point.
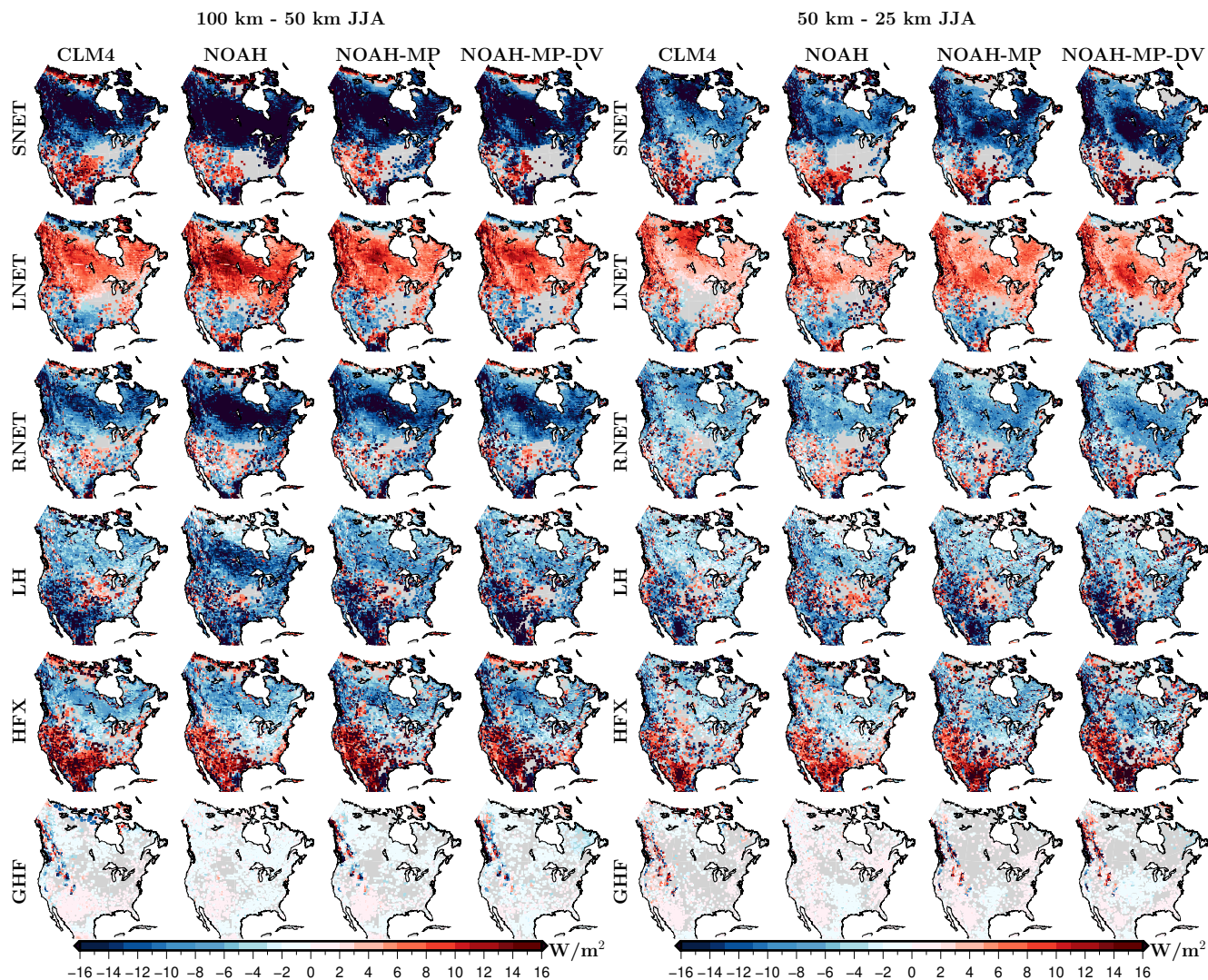
Figure S9. JJA mean difference in surface energy fluxes between the 100 km and 50 km simulations (left) and between the 50 km and 25 km simulations (right). Grid cells with a non-significant change at the 5% significant level are masked in grey. All outputs from the 25, 50 and 100 km simulations were mapped to a common grid (CRU grid) using the nearest model grid point.
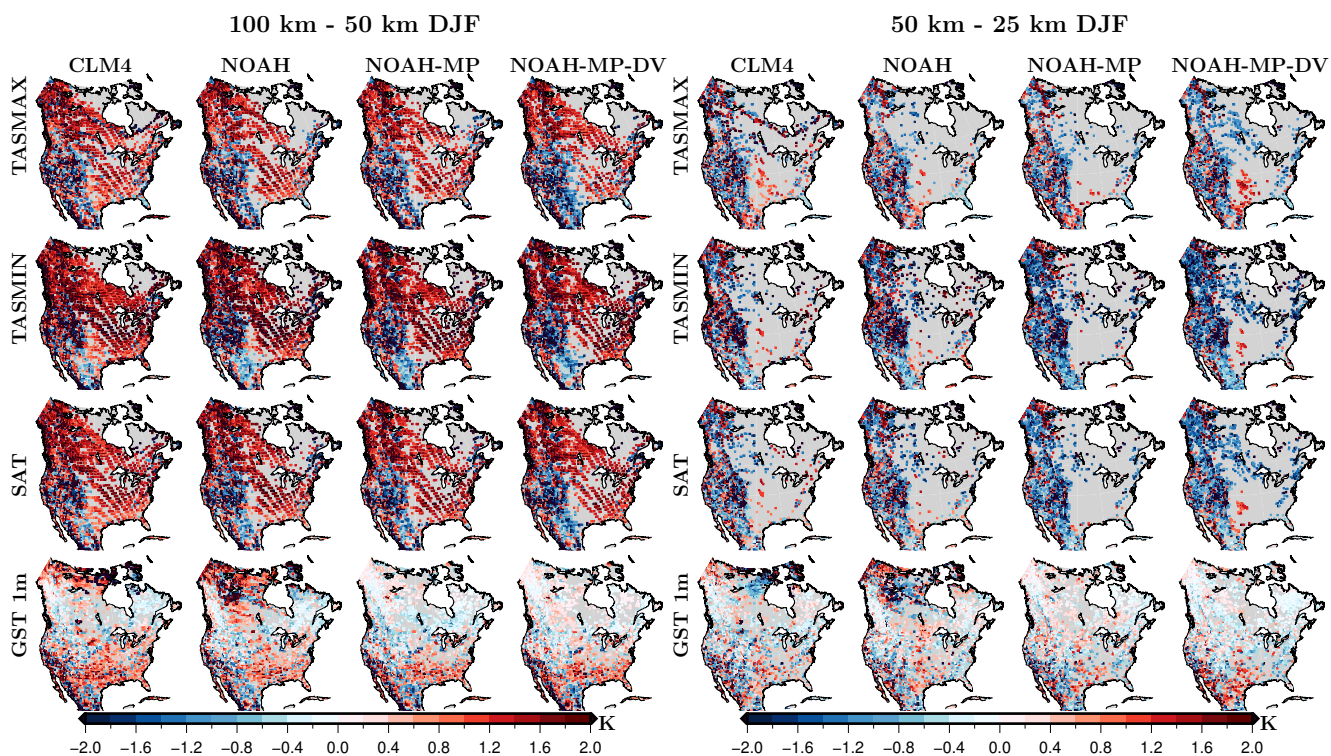
Figure S10. DJF mean difference in near-surface temperature conditions between the 100 km and 50 km simulations (left) and between the 50 km and 25 km simulations (right). Grid cells with a non-significant change at the 5% significant level are masked in grey. All outputs from the 25, 50 and 100 km simulations were mapped to a common grid (CRU grid) using the nearest model grid point.
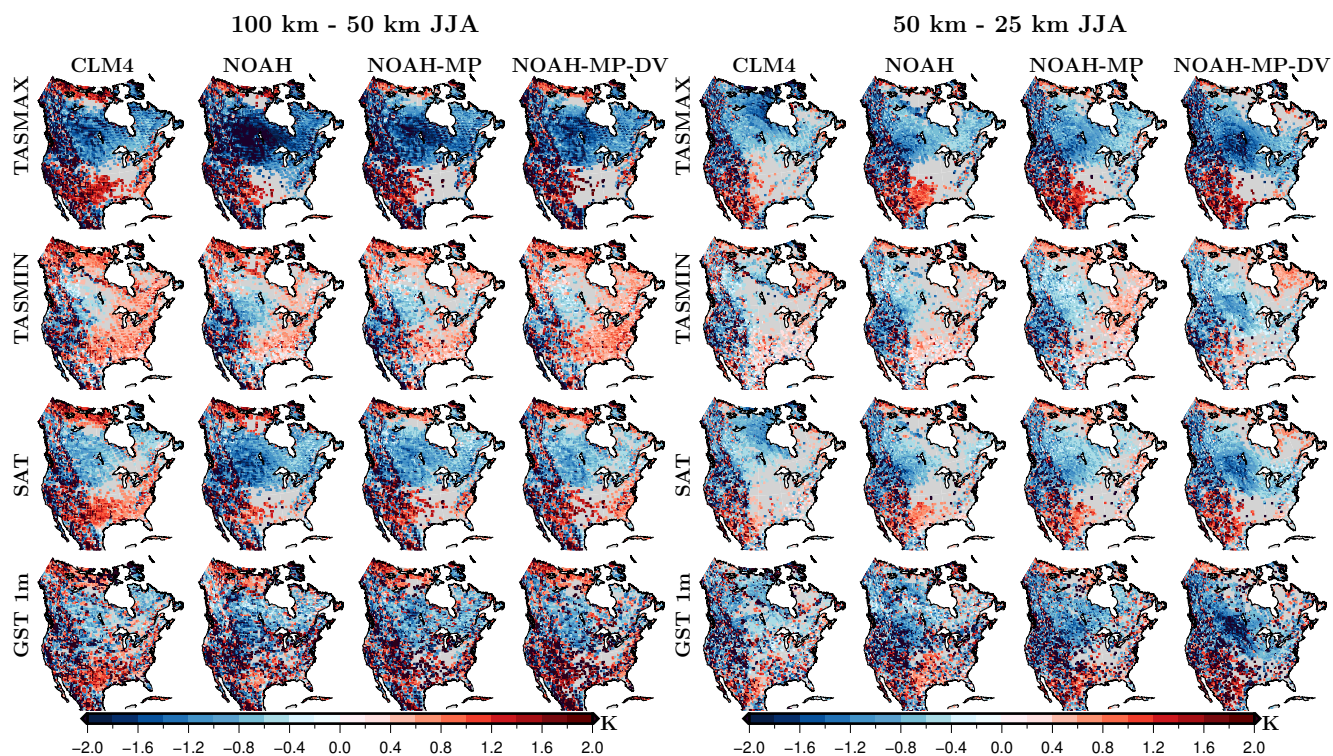
Figure S11. JJA mean difference in near-surface temperature conditions between the 100 km and 50 km simulations (left) and between the 50 km and 25 km simulations (right). Grid cells with a non-significant change at the 5% significant level are masked in grey. All outputs from the 25, 50 and 100 km simulations were mapped to a common grid (CRU grid) using the nearest model grid point.
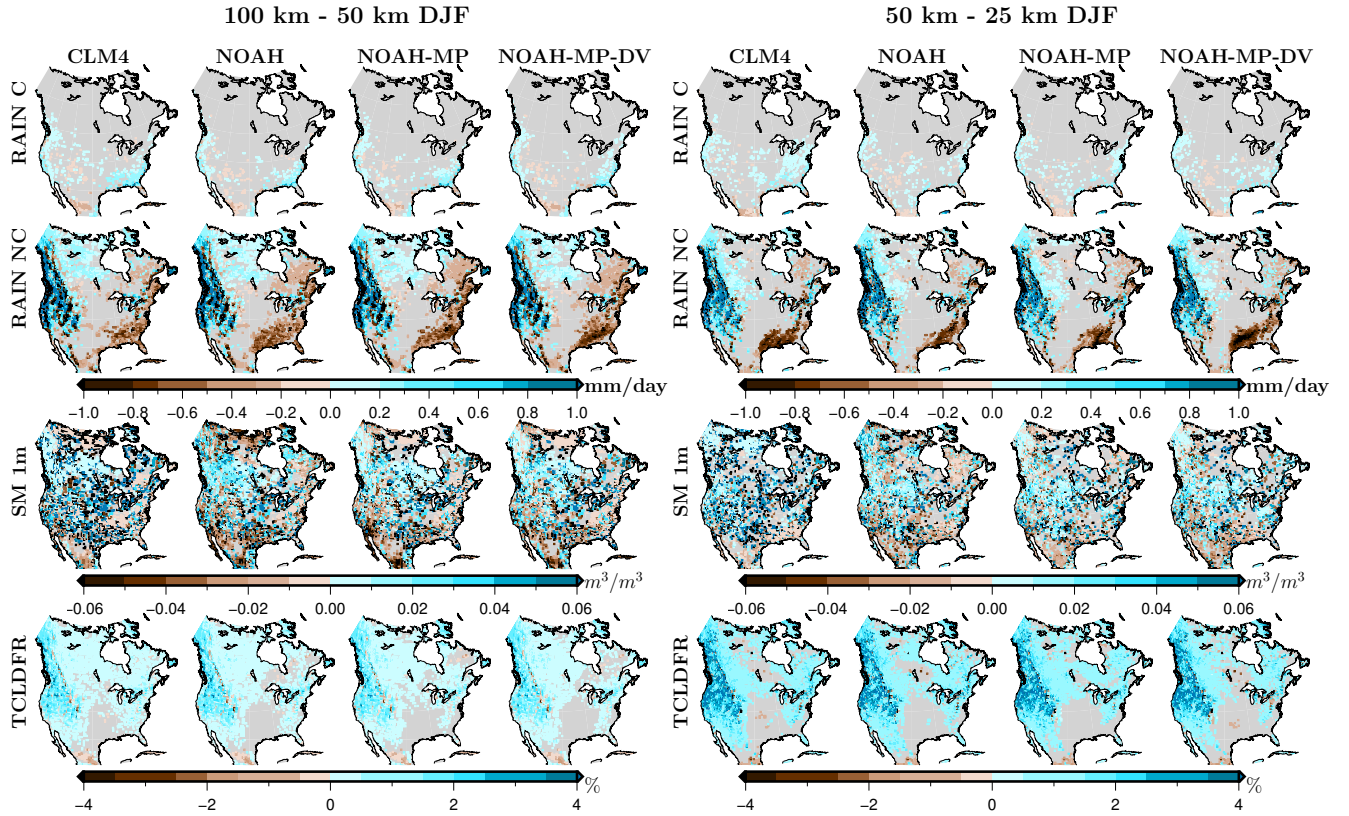
Figure S12. DJF mean difference in near-surface humid conditions between the 100 km and 50 km simulations (left) and between the 50 km and 25 km simulations (right). All outputs are from the NOAH-MP-DV simulations for the period 1980-2013. Grid cells with a non-significant change at the 5% significant level are masked in grey. All outputs from the 25, 50 and 100 km simulations were mapped to a common grid (CRU grid) using the nearest model grid point.
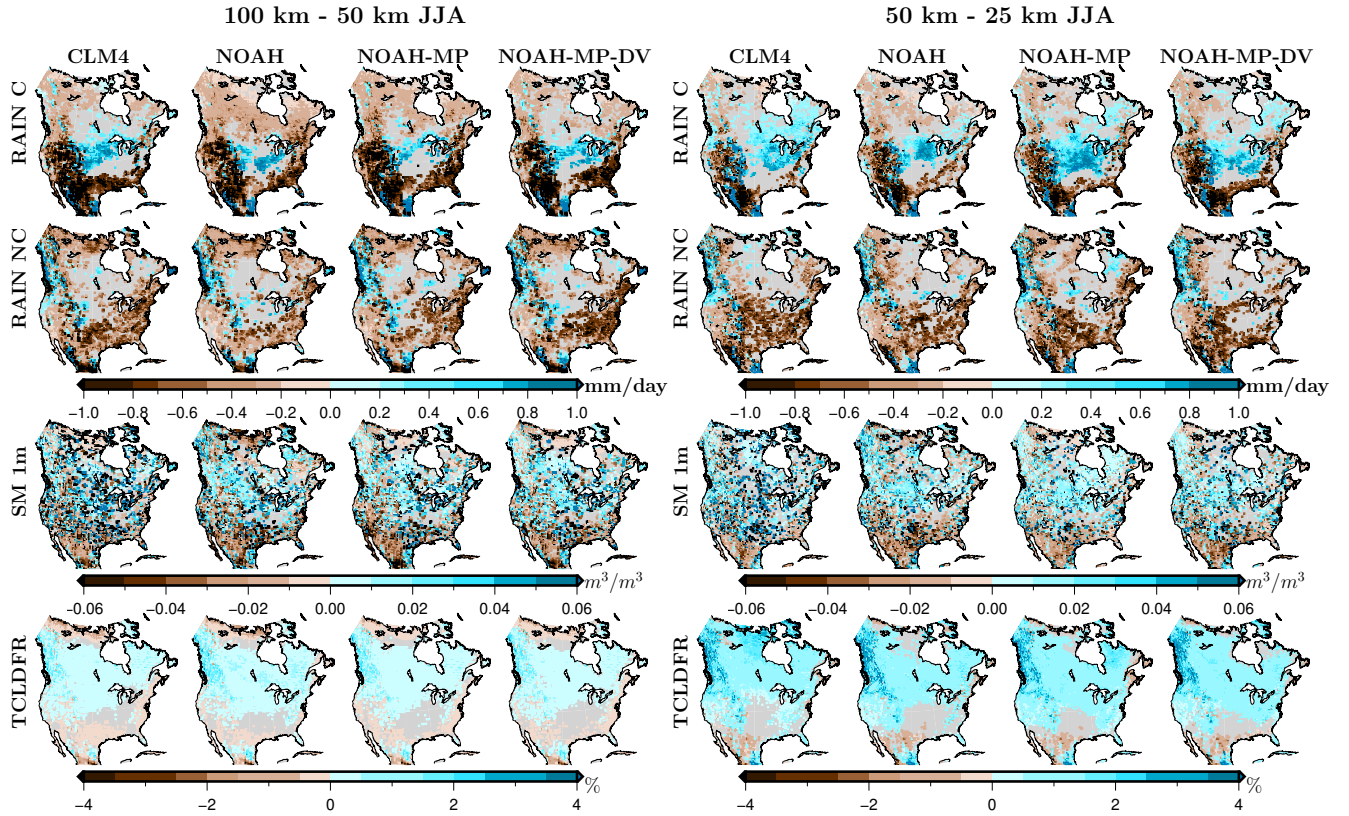
Figure S13. JJA mean difference in near-surface humid conditions between the 100 km and 50 km simulations (left) and between the 50 km and 25 km simulations (right). All outputs are from the NOAH-MP-DV simulations for the period 1980-2013. Grid cells with a non-significant change at the 5% significant level are masked in grey. All outputs from the 25, 50 and 100 km simulations were mapped to a common grid (CRU grid) using the nearest model grid point.
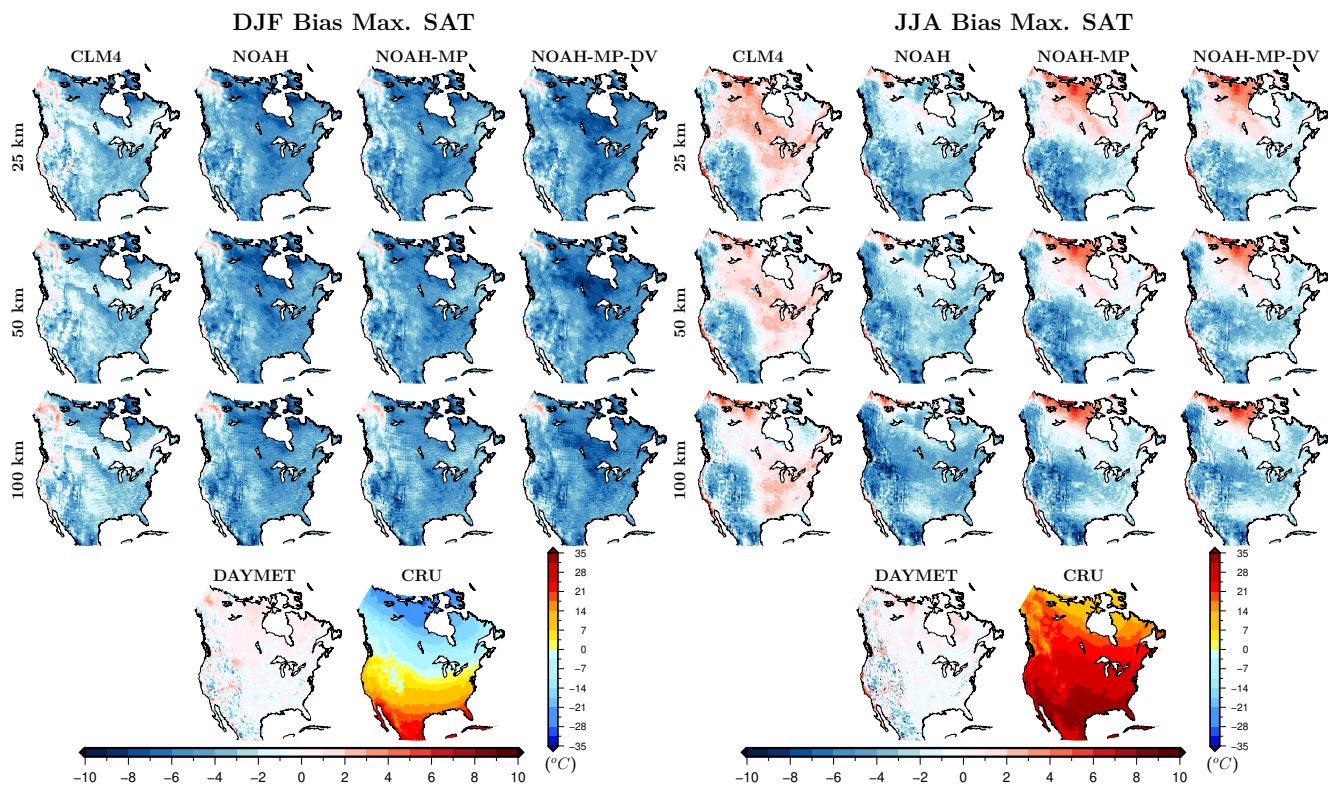
Figure S14. DJF (left) and JJA (right) bias in maximum temperature (^oC) for all experiments and the DAYMET data product relative to the CRU database from 1980 to 2013. Grid cells with a non-significant change at the 5% significant level are masked in grey. All outputs were mapped to a common grid (CRU grid) using the nearest model grid point.
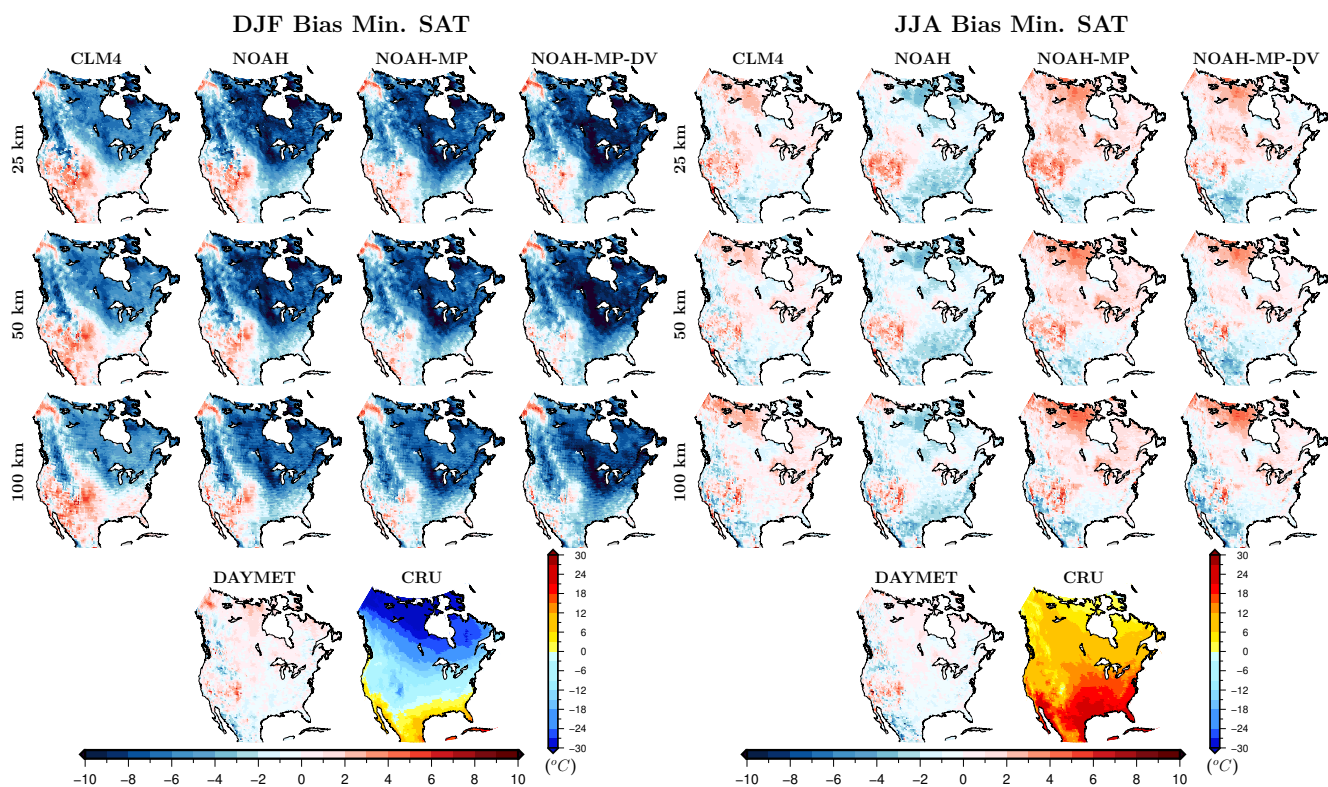
Figure S15. DJF (left) and JJA (right) bias in minimum temperature (^{o}C) for all experiments and the DAYMET data product relative to the CRU database from 1980 to 2013. Grid cells with a non-significant change at the 5% significant level are masked in grey. All outputs were mapped to a common grid (CRU grid) using the nearest model grid point.
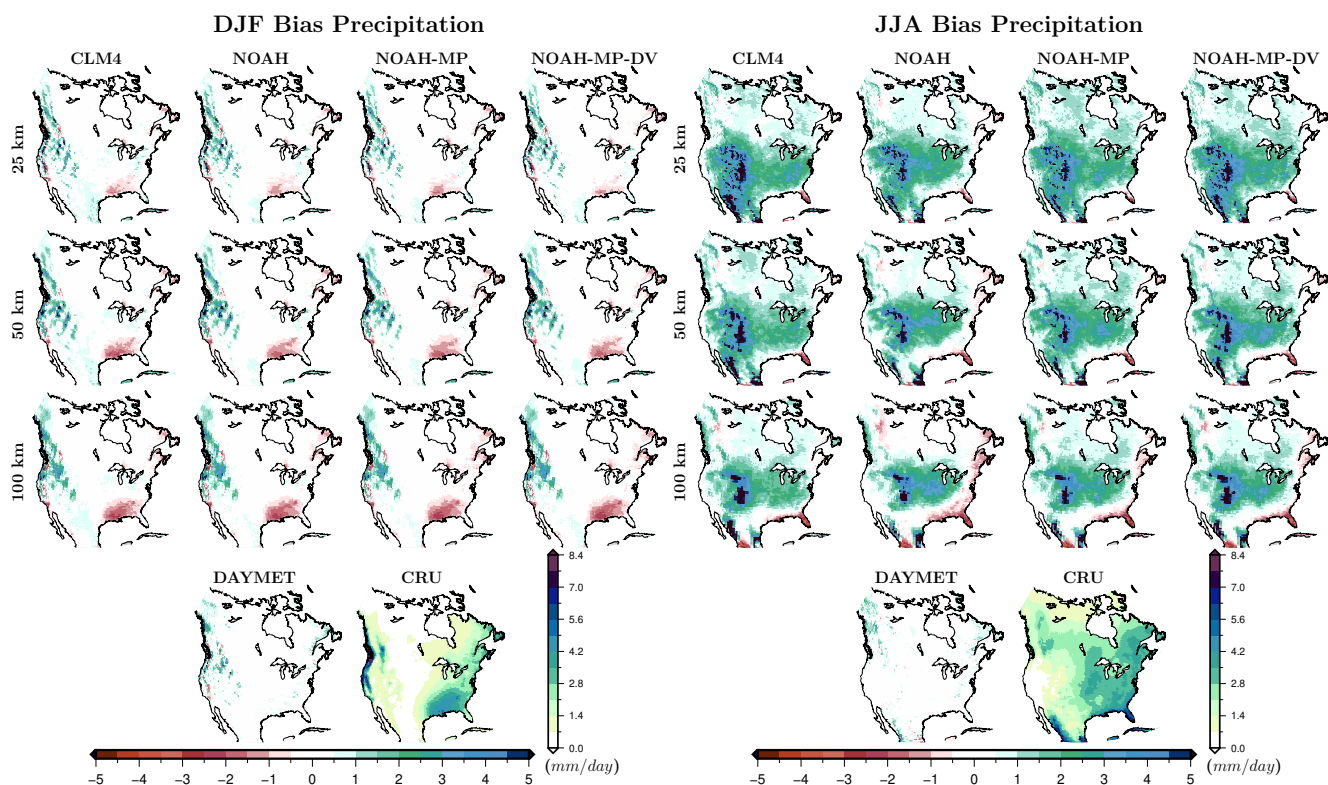
Figure S16. DJF (left) and JJA (right) bias in accumulated precipitation (mm/day) for all experiments and the DAYMET data product relative to the CRU database from 1980 to 2013. Grid cells with a non-significant change at the 5% significant level are masked in grey. All outputs were mapped to a common grid (CRU grid) using the nearest model grid point.